Atmos. Chem. Phys. Discuss., 13, 21883–21926, 2013
www.atmos-chem-phys-discuss.net/13/21883/2013/
doi:10.5194/acpd-13-21883-2013

Atmospheric Chemistry and Physics Discussions
Open Access

Quantifying global terrestrial methanol emissions using observations from the TES satellite sensor

K. C. Wells[1], D. B. Millet[1], K. E. Cady-Pereira[2], M. W. Shephard[3], D. K. Henze[4], N. Bousserez[4], E. C. Apel[5], J. de Gouw[6,7], C. Warneke[6,7], and H. B. Singh[8]

[1]Department of Soil, Water, and Climate, University of Minnesota, St. Paul, Minnesota, USA
[2]Atmospheric and Environmental Research, Inc., Lexington, Massachusetts, USA
[3]Environment Canada, Downsview, Ontario, Canada
[4]Department of Mechanical Engineering, University of Colorado at Boulder, Boulder, Colorado, USA
[5]Atmospheric Chemistry Division, NCAR, Boulder, Colorado, USA
[6]Earth System Research Laboratory, NOAA, Boulder, Colorado, USA
[7]CIRES, University of Colorado, Boulder, Colorado, USA
[8]NASA Ames Research Center, Moffett Field, California, USA

Received: 21 June 2013 – Accepted: 15 August 2013 – Published: 23 August 2013

Correspondence to: D. B. Millet (dbm@umn.edu)

Published by Copernicus Publications on behalf of the European Geosciences Union.

Abstract

We employ new global space-based measurements of atmospheric methanol from the Tropospheric Emission Spectrometer (TES) with the adjoint of the GEOS-Chem chemical transport model to quantify terrestrial emissions of methanol to the atmosphere. Biogenic methanol emissions in the model are based on MEGANv2.1 emission algorithms, using MODIS leaf area and GEOS-5 assimilated meteorological fields. We first carry out a pseudo observation test to validate the overall approach, and find that the TES sampling density is sufficient to accurately quantify regional- to continental-scale methanol emissions using this method. A global inversion of two years of TES data yields an optimized annual global surface flux of 117 Tg yr^{-1} (including biogenic, pyrogenic, and anthropogenic sources), an increase of 56 % from the a priori global flux of 75 Tg yr^{-1}. Global terrestrial methanol emissions are thus approximately 25 % those of isoprene ($\sim$540 Tg yr^{-1}), and are comparable to the combined emissions of all anthropogenic volatile organic compounds ($\sim$100–200 Tg yr^{-1}). Our a posteriori terrestrial methanol source leads to a strong improvement of the simulation relative to an ensemble of airborne observations, and corroborates two other recent top-down estimates (114–120 Tg yr^{-1}) derived using in-situ and space-based measurements. The TES data imply a relatively modest revision of model emissions over most of the tropics, but a significant upward revision in midlatitudes, particularly over Europe and North America. We interpret the inversion results in terms of specific source types using the methanol:CO correlations measured by TES, and find that biogenic emissions are overestimated relative to biomass burning and anthropogenic emissions in central Africa and southeastern China, while they are underestimated in regions such as Brazil and the US. Based on our optimized emissions, methanol accounts for >25 % of the photochemical source of CO and HCHO over many parts of the northern extratropics during springtime, and contributes $\sim$6 % of the global secondary source of those compounds annually.

1 Introduction

Methanol is the most abundant non-methane organic compound in the troposphere, and a precursor of carbon monoxide, formaldehyde, and ozone (Singh et al., 1995, 2001; Tie et al., 2003; Millet et al., 2006; Duncan et al., 2007; Choi et al., 2010; Hu et al., 2011). Methanol is produced in plants during cell wall growth (Fall, 2003), and appears to be emitted by most land plants (Fall and Benson, 1996). As a result, biogenic emissions are thought to constitute the largest fraction of the global source (Millet et al., 2008a; Stavrakou et al., 2011; Guenther et al., 2012). Emissions of methanol thus represent an important chemical interaction between the biosphere and atmosphere.

Other sources of atmospheric methanol include biomass burning (Holzinger et al., 1999; Andreae and Merlet, 2001) and anthropogenic emissions (Holzinger et al., 1999; de Gouw et al., 2005; Hu et al., 2011), both minor terms in the global budget that can be important on regional scales. Methanol is also produced photochemically via peroxy radical permutation reactions (Tyndall et al., 2001), which provide a diffuse source most important in the remote atmosphere (Lewis et al., 2005). Observations in the ocean mixed layer imply that the marine biosphere is a large primary source of atmospheric methanol, but an even larger gross sink (Heikes et al., 2002; Williams et al., 2004; Carpenter et al., 2004; Millet et al., 2008a). Photochemical oxidation by the hydroxyl radical (OH) is the other main sink for atmospheric methanol, followed by dry deposition to land. The overall atmospheric lifetime for methanol, accounting for gross ocean uptake, OH, and deposition, is approximately 5–6 days (Millet et al, 2008b; Stavrakou et al., 2011).

Due to sparse long-term surface observations, the magnitude and distribution of global methanol sources is poorly constrained. Recent studies have found that current emission inventories lead to significant spatial and temporal model biases relative to in-situ and satellite observations. Millet et al. (2008b) found that a net primary productivity-(NPP-) based emissions scheme developed by Galbally and Kirstine (2002), implemented in a chemical transport model (GEOS-Chem CTM), led to a methanol overprediction over the eastern US and the tropics that correlated with broadleaf tree coverage. Stavrakou et al. (2011) used methanol column measurements from the Infrared Atmospheric Sounding Interferometer (IASI) with the adjoint of the IMAGESv2 CTM to constrain biomass burning and biogenic methanol emissions globally. They found that the Model of Emissions of Gases and Aerosols from Nature (MEGANv2.1; Guenther et al., 2012) predicted biogenic methanol emissions that were too high in the tropics, and too low in more arid regions such as the western US, central Asia, and northern Australia.

Hu et al. (2011) employed tall tower measurements in the US Upper Midwest in combination with the GEOS-Chem CTM to better understand the seasonal cycle of methanol emissions. They showed that methanol concentrations simulated by GEOS-Chem, driven by MEGANv2.1, peaked a month too late in summer compared to the observations (late July versus June). This led in turn to an underestimate of the photochemical importance of methanol in early spring, when methanol emissions are high but isoprene emissions are still relatively low. Wells et al. (2012) used space-based measurements from IASI and from the Tropospheric Emission Spectrometer (TES) to demonstrate that this seasonal bias manifests across midlatitude ecosystems globally. They used the IASI data to derive an optimized set of emission factors as a function of leaf age, which resulted in higher emissions for new and old leaves, and reduced emissions from growing and mature leaves, relative to the standard MEGAN parameterization.

In this paper, we use a new 2-year dataset of space-based tropospheric methanol observations from TES with the adjoint of the GEOS-Chem CTM in a global inversion to derive new constraints on terrestrial emissions of methanol. The analysis builds on our previous work using satellite observations to characterize the seasonality of methanol emissions in the extratropics (Wells et al., 2012), and on recent efforts applying the IASI sensor to investigate global emission fluxes (Stavrakou et al., 2011). We employ an ensemble of aircraft observations to evaluate the TES-derived emission estimates, and interpret the results in terms of underlying emission processes based on the methanol:CO correlations measured by TES. Finally, we explore the impact of our a posteriori methanol emissions on the photochemical production of formaldehyde and carbon monoxide in the global troposphere.

2 TES methanol observations

TES is an infrared Fourier transform spectrometer onboard EOS Aura, which has a local equator overpass time of 13:45 and a $5 \times 8\,\mathrm{km}^2$ footprint at nadir (Beer et al., 2001). The first observations of methanol from TES were presented in Beer et al. (2008), and a detailed description of the methanol retrieval, sensitivity, and initial global results were given by Cady-Pereira et al. (2012). Wells et al. (2012) evaluated the TES retrievals using a suite of aircraft observations over North America, and found the two datasets to be consistent for retrievals with degrees of freedom for signal (DOFS) > 0.5.

The methanol abundance is retrieved from TES measured spectra in the band ranging from 1032.32 to $1034.48\,\mathrm{cm}^{-1}$ using an optimal estimation approach (Rodgers, 2000). The retrieved methanol profile is related to the true profile $\boldsymbol{x}$ by

$$\widehat{\boldsymbol{x}} = \boldsymbol{x}_a + \mathbf{A}(\boldsymbol{x} - \boldsymbol{x}_a) \quad (1)$$

where $\boldsymbol{x}_a$ is the a priori profile and $\mathbf{A}$ is the averaging kernel matrix. Most TES methanol retrievals have DOFS < 1.0, so they contain at most one piece of information in the vertical. Because of this, we collapse the retrieved methanol profile into a single mixing ratio, called the representative volume mixing ratio (RVMR; Shephard et al., 2011). The RVMR (ρ) is a measure of the methanol concentration over the vertical range where TES is most sensitive, and is calculated from the retrieved profile as:

$$\rho = \exp\left[\sum_{i=1}^{n_{\mathrm{levs}}} \log(\widehat{x}_i)\, w_i\right] \quad (2)$$

where $\widehat{x}_i$ and w_i are the retrieved mixing ratio and RVMR weighting function at level i. The weighting function is derived from a transformation of the averaging kernel, and reduces to a vector in cases where the information content of the retrieval is limited (DOFS < 1.0). The uncertainty of the methanol RVMR typically ranges from 10 to 50 %. The sensitivity of the retrieval to the true methanol profile peaks in the lower troposphere, typically between 700 and 900 hPa (Cady-Pereira et al., 2012), making the TES data suitable for investigating surface emissions.

Here, we employ the GEOS-Chem 3-D CTM (see below) to interpret two years of global methanol observations from TES in terms of the constraints they provide on methanol emission processes. We restrict the analysis to retrievals over land and where the surface emissivity is greater than 0.92, which results in 62,209 retrieved profiles from 2008 and 2009. The number of TES observations per GEOS-Chem grid box, and their average DOFS, are mapped in Fig. 1 for the full data record and for the months of January and July. We see in Fig. 1a that TES provides extensive data coverage in the tropics, but relatively few observations over North Africa, the Arabian Peninsula, and much of Australia. The latter are desert regions where the surface emissivity retrieval degrades in accuracy due to a strong and variable silicate absorption feature between 800 and 1300 cm^{-1}. Errors in the emissivity retrieval can overwhelm the methanol signal over these areas. We also see in Fig. 1a-b that the number of observations and their corresponding DOFS decrease towards the poles, particularly in the Northern Hemisphere (NH). This mainly arises from the sparse observations during wintertime (Fig. 1c). During NH spring and summer, when methanol concentrations are elevated and there is greater thermal contrast between the land and atmosphere, we obtain more TES observations (and increased DOFS) at higher latitudes (Fig. 1e–f).

To compare the simulated and measured methanol profiles in the adjoint optimization, we sample the model at the time and location of each TES observation, interpolate the model profile to the TES vertical resolution, and apply the native TES a priori and averaging kernel using Eq. (1). The model-measurement difference is then used to compute the adjoint forcing profile in the inversion, as described in the following section.

3 Methanol simulation in the GEOS-Chem CTM

GEOS-Chem (http://www.geos-chem.org) is a global, 3-D model of atmospheric chemistry that uses GEOS-5 assimilated meteorological data from the NASA Goddard Earth Observing System. For this work we run the model at a horizontal resolution of 4° × 5° and with 47 vertical levels extending to 0.01 hPa. Transport and emissions are calculated on 30 and 60 min time steps, respectively.

Methanol sources and sinks are computed in the model following Millet et al. (2008b), with modifications described in Wells et al. (2012). Specifically, terrestrial biogenic emissions are estimated using the MEGANv2.1 algorithms (Guenther et al., 2012), with the seasonality in the extratropics updated to provide better agreement with atmospheric measurements (Wells et al., 2012), and using climatological monthly leaf area indices (LAI) from MODIS collection 5 (Yang et al., 2006). Biomass burning emissions are calculated based on monthly output from the GFEDv3 database (van der Werf et al., 2010). The methanol air-sea flux calculation derives the gas-phase and liquid-phase transfer velocities using the parameterizations of Johnson et al. (2010) and Nightingale (2000), respectively. Dry deposition of methanol includes reactive uptake by vegetation as recommended by Karl et al. (2010). The resulting annual methanol source in our a priori simulation is 179 $\mathrm{Tg\,yr^{-1}}$, with 64 $\mathrm{Tg\,yr^{-1}}$ from terrestrial plants, 36.5 $\mathrm{Tg\,yr^{-1}}$ from secondary photochemical production, 8 $\mathrm{Tg\,yr^{-1}}$ from biomass and biofuel burning, and 4.5 $\mathrm{Tg\,yr^{-1}}$ from anthropogenic activities. Gross methanol emissions from the ocean surface contribute 66 $\mathrm{Tg\,yr^{-1}}$, but annual gross ocean uptake of 73.5 $\mathrm{Tg\,yr^{-1}}$ results in a net ocean sink of 7.5 $\mathrm{Tg\,yr^{-1}}$. Other sinks in the a priori simulation include oxidation by OH (70 $\mathrm{Tg\,yr^{-1}}$), dry deposition to land (26 $\mathrm{Tg\,yr^{-1}}$), and wet deposition (9.5 $\mathrm{Tg\,yr^{-1}}$).

For this work we run the model for year-2008, and use a one-year spin up to minimize any impact from initial conditions. To increase data coverage, we then compare the model output to TES retrievals for 2008 and 2009, under the assumption that interannual variability is smaller than other sources of model error (globally, terrestrial fluxes differ by less than 1 % for the two years in the a priori simulation).

Figure 2 maps the annual terrestrial methanol emissions in the GEOS-Chem a priori simulation. Fluxes are highest in the tropics, where emissions from terrestrial plants and biomass burning peak. Our a priori emission estimate for terrestrial plants in 2008 is ~35 % lower than the 99.6 Tg yr^{-1} reported by Guenther et al. (2012) for the year 2000, likely due primarily to the use of differing LAI and meteorological drivers.

4 GEOS-Chem adjoint

We carry out an inverse analysis to quantitatively constrain global terrestrial methanol emissions on the basis of the TES data. The method involves minimizing a scalar cost function, $J(\boldsymbol{p})$, that quantifies the error weighted misfit of the model to the TES observations while accounting for prior knowledge:

$$J(\boldsymbol{p}) = \frac{1}{2}\sum_{c\in\Omega}(\mathbf{H}(c) - \boldsymbol{y})^T\mathbf{S}_y^{-1}(\mathbf{H}(c) - \boldsymbol{y}) + \frac{1}{2}\gamma(\boldsymbol{p} - \boldsymbol{p}_a)^T\mathbf{S}_a^{-1}(\boldsymbol{p} - \boldsymbol{p}_a) \quad (3)$$

Here, $\boldsymbol{p}$ is the vector of parameters (in our case, scale factors for terrestrial emissions) to be optimized, $\boldsymbol{p}_\mathbf{a}$ is their initial (a priori) value, $\boldsymbol{y}$ is a set of observations (in our case, TES methanol profiles), $\boldsymbol{c}$ is a vector containing the model-simulated concentrations, $\mathbf{H}$ is an observation operator mapping from the model space to the observation space, $\mathbf{S}_y$ is the observational error covariance matrix, $\mathbf{S}_a$ is the a priori emissions error covariance matrix, and Ω is the time and space domain of the observations. We also include a γ term to help regularize the solution to this problem given a lack of complete knowledge of the error statistics of the a priori emissions (Hansen, 1998). The maximum a posteriori solution for $\boldsymbol{p}$ is then given by the solution to min $(J(\boldsymbol{p}))$.

For this work we use the GEOS-Chem adjoint to solve for min$(J(\boldsymbol{p}))$. The model adjoint computes the gradient of $J(\boldsymbol{p})$ with respect to methanol emissions, and employs a quasi-Newtonian optimization routine to iteratively converge to $\nabla_\mathbf{p}J(\boldsymbol{p}) = 0$ (Zhu et al., 1994; Byrd et al., 1995). Previous applications of the GEOS-Chem adjoint have included inverse modeling and sensitivity studies focused on aerosols (Henze et al., 2009; Kopacz et al., 2011; Wang et al., 2012), CO (Kopacz et al., 2009, 2010), NH_3 (Zhu et al., 2103), and O_3 (Zhang et al., 2009; Parrington et al., 2012), with additional studies developing complete error covariance constraints (Singh et al., 2011) and quantifying the impact of model error on inverse calculations (Jiang et al., 2011, 2013).

Our optimization employs two years of TES methanol profiles to derive terrestrial emissions at $4^\circ \times 5^\circ$, including the sum of contributions from anthropogenic activities, biofuel and biomass burning, and terrestrial plants. The TES data have greater coverage over the tropics (Fig. 1). Since the seasonal cycle of extra-tropical emissions in the model is already well constrained based on our earlier work (Wells et al., 2012), we perform here a seasonal inversion in the tropics (December–February, March–May, June–August, and September–November; hereafter DJF, MAM, JJA, and SON), defined as 23.5° S to 23.5° N, and an annual inversion in the extratropics. We exclude retrievals over oceans, as these tend to have limited information content due to weak thermal contrast and low methanol abundance. The optimization routine bounds the solution so that the optimized emission scale factors are not less than zero, and the a priori emissions are assumed to have an uncertainty of 100 % (with $\gamma = 0.5$).

The observational error is calculated from the native TES instrument noise error covariance matrix (diagonal elements only); we apply a minimum threshold of 0.5 ppb for this error as this corresponds to the TES limit of detection for the methanol RVMR (Cady-Pereira et al. 2012). We add to this an assumed 20 % CTM error following Millet et al. (2012). An example TES retrieved profile, model profile (with TES averaging kernel and a priori profile applied), TES averaging kernel, and the corresponding adjoint forcing profile ($\partial J/\partial \boldsymbol{p}$) with respect to the a priori emissions are shown in Fig. 3. The adjoint forcing in this case is strongest around 600 hPa, and is negative as the model concentrations are lower than the retrieved values for this example.

5 Pseudo observation test of the adjoint method

We performed a sensitivity analysis using pseudo observations to determine the spatial resolution at which the TES data can be expected to constrain surface emissions of methanol. The GEOS-Chem methanol fields were sampled according to the temporal and spatial sampling density of the two-year TES dataset, and the native TES a priori profiles and averaging kernels then applied to the model output using Eq. (1) to generate pseudo-TES observations. We then carried out two global adjoint inversions using these pseudo-TES observations: one with the a priori estimate for terrestrial emissions perturbed downward (0.5 ×) from their actual values, and one with the estimate perturbed upward (1.5 ×). Ideally the adjoint optimization would be able to recover the actual model emissions in each grid square; the degree to which this is not the case provides a measure of the uncertainty arising from the TES data coverage.

Figures S1 and S2 show the a posteriori emission scale factors for these test inversions. For both tests, there are a number of model grid boxes with optimized scale factors that are higher or lower than 1.0, showing that the TES data sampling provides some limitation on our ability to retrieve emissions for any individual grid box. On the other hand, when we aggregate to larger regions, we find that the derived emissions are robust. Table 1 lists the optimized emissions, normalized by their true values and averaged over continental-scale regions (with boundaries as in Fig. S3). At this scale, the retrieved emissions for most regions are within 10 % of the actual values. Emissions in regions encompassing Siberia and Indonesia/Oceania have somewhat higher uncertainty (15–25 %), due to a limited number of TES observations.

In the following section, we use these same regions for interpreting the terrestrial methanol emissions derived from the actual TES measurements.

6 Optimized methanol sources

Figure 4 shows the evolution of the cost function during the optimization of terrestrial methanol emissions using the actual TES observations, and Fig. 5 shows the corresponding scale factors for the a priori emission estimates. We converge on a solution after approximately 26 iterations, with the a posteriori cost function reduced by ∼31 % compared to the a priori value.

Figure 5 reveals some coherent and informative spatial patterns. Several of the regions where emissions are revised significantly upward are semi-arid, such as the western US and Mexico, the Iberian Peninsula, the Sahel, and central Asia. This is consistent with the findings of Stavrakou et al. (2011), who used IASI methanol retrievals to test MEGANv2.1 biogenic emissions in the IMAGESv2 model.

The optimization also leads to increased emission estimates for the eastern US, western Canada, eastern Africa, South Africa, and most of South America. Emissions from Brazil are revised upward during SON. A particular region where emissions are scaled downward is central Africa (mainly in JJA); emissions are also reduced in southeastern China and southeastern Russia.

We saw based on the pseudo-observation analysis in the previous section that the inversion is more robust across regional scales than it is for individual grid boxes. Figure 6 maps the a posteriori uncertainties for the actual inversion (calculated using a preconditioned BFGS algorithm; Bousserez et al., 2013), which provide a more nuanced picture of the spatial constraints afforded by the optimization. We see in Fig. 6 that the a priori error is reduced by half throughout most of the northern midlatitudes, and by over 70 % in portions of Europe, East Asia, Central Africa, and Brazil (in SON). The DOFS for our inversion (which indicate the number of independently constrained emission variables) are 547.

Table 2 lists our optimized terrestrial methanol emission estimates for continental-scale regions around the world. Although there are parts of the tropics where emissions are reduced relative to the a priori estimate (Fig. 5), when aggregated to continental scales the a posteriori emissions are uniformly higher than the a priori. The global terrestrial methanol emission flux increases by 56 % in the inversion, from 76 to 117 Tg yr^{-1} for the 2008–2009 period. This revised estimate supports two other recent top-down estimates of the global terrestrial methanol source: 114 Tg yr^{-1} for 2009 (Stavrakou et al., 2011) and 120 Tg yr^{-1} for 2004 (Millet et al., 2008a). Including gross ocean emissions of 66 Tg yr^{-1} and secondary photochemical production totaling 36.5 Tg yr^{-1}, the total global methanol source increases by 24 % as a result of the inversion. Relative emission increases are highest over Europe and North America (125–175 % increase over the a priori emissions) followed by Southeast Asia/India and Siberia. The smallest relative changes occur over Central/Southern Africa, South America, and Indonesia/Oceania (Table 2).

Figure 7 shows TES RVMR annual timelines, averaged over 2008–2009 for the continental-scale regions mapped in Fig. S3. We also show timelines for Brazil and central Africa (with outlines as indicated by the green boxes in Fig. S3) to better assess the impact of the seasonal optimization in the tropics. Since the adjoint inversion was driven by the TES data, these comparisons are not an independent validation of the results, but instead provide a regional and seasonal comparison of the a priori and a posteriori simulations. Note that the optimization employed the full TES profile rather than just the RVMR values summarized in Fig. 7.

As we see in Fig. 7, the optimized simulation achieves significantly better agreement with the TES observations across these different global regions. Some discrepancies do persist. The simulated methanol RVMRs over Southeast Asia/India, Central/South Africa, and Indonesia/Oceania are still somewhat underestimated in the optimized simulation throughout the year, and wintertime concentrations are underestimated over North America, Europe, and Siberia. The latter behavior is probably due to the limited number of TES observations at higher latitudes in wintertime. In the tropics, the optimized simulation is better able to capture both the seasonal cycle and magnitude of observed methanol concentrations than is the a priori simulation.

7 Sensitivity analyses

Although we have included only terrestrial emissions in our state vector for optimization, other model processes, such as the methanol loss rate, might also contribute to the observed model-measurement discrepancies. In particular, a body of recent research has pointed to large inconsistencies between simulated and measured OH levels over high-isoprene, low-NO_x environments such as tropical forests (Lelieveld et al., 2008; Kubistin et al., 2010; Pugh et al., 2010; Stone et al., 2011). We performed a suite of sensitivity runs to assess the degree to which such uncertainties in model OH are likely to affect our derived emission fluxes. First, we repeated the inversion using global oxidant fields from a different version of GEOS-Chem, corresponding to a 6.4 % lower global OH burden than the standard simulation (Millet et al., 2012). Next, we implemented a parameterization (denoted p3OH) that has been proposed by Stone et al. (2011) to approximate OH recycling during isoprene oxidation under low-NO_x conditions (i.e., assuming that 3.0 OH radicals are produced for each OH radical lost to isoprene).

Table 2 gives a summary of the inversion results for these sensitivity runs. The a posteriori emissions are very similar for the inversions using the two alternate OH fields derived using standard model isoprene chemistry. The OH recycling tests do impact the optimized fluxes to a degree in the tropics. Over central Africa, optimized emissions for the p3OH simulation are 25 % higher than they are when the standard model chemistry is used in the inversion. Over Brazil, optimized emissions are about 28 % higher for the p3OH simulation.

Mao et al. (2012) argue that, to some extent, measurement uncertainties may have contributed to reported observation-model OH discrepancies in forest atmospheres. As such, we take the p3OH parameterization as an OH-recycling upper limit, and conclude that current uncertainties in low-NO_x isoprene chemistry likely lead to at most a 30 % uncertainty in our derived tropical methanol emissions. Likewise, Table 2 shows that use of the alternate global OH fields leads to at most a 10 % change in our derived continental-scale methanol emission fluxes.

We also tested the extent to which our a priori constraint impacts the optimized emissions. In addition to the baseline inversion with $\gamma = 0.5$ (and overall a priori uncertainty = 100 %), we performed three sensitivity inversions with the regularization parameter set to 1.0, 0.01, and 0. The former two values correspond to an overall a priori uncertainty of ∼70 % and ∼700 %, respectively, while the third case contains no a priori constraint. The results indicate that our continental-scale emission fluxes are robust to assumptions regarding the a priori constraint. North America exhibits the greatest sensitivity, with the a posteriori continental emissions differing by ∼ 7 % between the baseline analysis and the no-constraint case; all other regions exhibit changes of less than 5 %.

8 Evaluation of optimized methanol sources using aircraft data

In this section we use an ensemble of in situ measurements from recent aircraft campaigns to evaluate our new top-down estimates of terrestrial methanol emissions derived using TES. The aircraft campaigns include the International Transport and Chemical Transformation of Anthropogenic Pollution, ITCT-2K2 (Parrish et al., 2004) and ITCT-2K4 (Fehsenfeld et al., 2006); Megacity Initiative: Local and Global Research Observations, MILAGRO (Singh et al., 2009); Intercontinental Transport Experiment-Phase B, INTEX-B (Singh et al., 2009); the second Texas Air Quality Study, TexAQS-II (Parrish et al., 2009); Arctic Research of the Composition of the Troposphere from Aircraft and Satellites, ARCTAS (Jacob et al., 2010); and Aerosol, Radiation, and Cloud Processes affecting Arctic Climate, ARCPAC (Brock et al., 2011). Because the TES observations employed here are for 2008 and 2009, we compare the aircraft data to a priori and a posteriori model simulations for 2008 sampled at the time-of-year and location of the aircraft observations.

Figure 8 shows campaign-average vertical profiles of methanol over land, measured onboard the aircraft and simulated by GEOS-Chem before and after optimization. The a priori emissions result in a significant model underestimate across North America, particularly in the boundary layer. The optimization leads to a strong improvement in the model-measurement comparisons across the ensemble of campaigns, with the observed profiles generally well-captured in the a posteriori simulation. In a few locations, the low bias is not entirely removed by the inversion. In particular, elevated boundary layer concentrations measured over the western US during INTEX-B and ARCTAS are not captured by the model. These campaigns both featured sampling over the California Central Valley and the Los Angeles area, where recent studies have found very high boundary layer concentrations of methanol (Warneke et al., 2010). High alcohol emissions from agricultural processes such as the fermentation of livestock feed have also been reported in this region (Howard et al., 2010; Malkina et al., 2011). Likewise, a residual low model bias is seen relative to the TexAQS-II measurements over Houston and the MILAGRO-C130 observations over and near Mexico City, probably because the flight data are heavily influenced by individual plumes that are not resolved at the $4^\circ \times 5^\circ$ model resolution. The DC8 observations during MILAGRO, representing more regional-scale outflow from Mexico City, are in good agreement with the optimized simulation.

Figure 9 shows marine methanol profiles for the above campaigns in which there was significant sampling over ocean. As before, the source optimization significantly improves the model agreement with the aircraft measurements throughout the vertical profile. The high free tropospheric methanol concentrations observed during INTEX-B over the eastern Pacific (C130 aircraft) are not captured by the model. A similar discrepancy was also noted by Stavrakou et al. (2011) relative to the IMAGESv2 CTM following an inversion using IASI data. On the other hand, our a posteriori simulation agrees well with other datasets over the Pacific and the Atlantic Oceans (Fig. 9), capturing the abundance of methanol for continental inflow to and outflow from North America.

9 Characterizing source contributions based on TES methanol:CO correlations

Our adjoint inversion optimized terrestrial methanol emissions as the sum of contributions from biogenic, biomass burning, and anthropogenic sources. In this section, we use methanol:CO correlations measured by TES to help interpret our inversion results in terms of specific source contributions. We select for the analysis regions that show significant differences between the a posteriori and a priori methanol emission estimates (Fig. S3). For the TES observations within each of the selected regions, we construct a methanol:CO correlation using methanol RVMR values and CO pseudo-RVMR values. The latter are computed by applying the TES RVMR weighting function for methanol to the corresponding retrieved CO profile using Eq. (2); this approach ensures consistent vertical weighting for both CO and methanol.

Figure 10 shows methanol:CO correlations measured by TES over the western US, eastern US, western Europe, and southeastern China (region boundaries are given in Fig. S3). Data are shown for June-August, corresponding to the seasonal peak in methanol concentrations in the NH extratropics, and include all retrievals with DOFS > 0.5. As we see from Fig. 5, the TES inversion leads to an upward revision of emissions for the western US, eastern US, and Europe, and a downward revision for southeastern China. The methanol:CO slopes are similar for the eastern US and western Europe (0.051–0.052 ppb ppb^{-1}), and both are lower than is observed over the western US (0.073 ppb ppb^{-1}). However, all three values are significantly higher than the enhancement ratios typically associated with anthropogenic emissions (~0.012 mol mol^{-1}; Goldan et al., 1995; de Gouw et al., 2005; Millet et al., 2005; Warneke et al., 2007), and this is consistent with the predominance of biogenic sources in the model for these regions during summer (Fig. 10). The higher slope over the western US shows that less of the methanol in this region is co-emitted with CO. The increased a posteriori emissions for this region could thus reflect the presence of plant species that emit large quantities of methanol, or a missing source from agriculture.

Over southeastern China, where the inversion leads to decreased emissions (Fig. 5), the methanol:CO slope is much lower (0.024 ppb ppb^{-1}), and closer to what would be expected for predominantly anthropogenic emissions. In contrast, the a priori methanol emissions over this region (Fig. 12) are mostly biogenic during the spring and summer months: it thus appears that the biogenic source for this region is overestimated.

Figure 11 shows the seasonal progression of methanol:CO correlations measured by TES over Brazil and central Africa, tropical regions where we expect a contribution from both biogenic and pyrogenic sources. Over Central Africa we see a distinct seasonal variation in the methanol:CO slopes, with lower values in JJA and DJF (0.017-0.023 ppb ppb^{-1}) compared to the other seasons (0.026–0.042 ppb ppb^{-1}). DJF and JJA correspond to the biomass burning seasons for this region (Fig. 11), and the observed slopes are in line with typical methanol:CO emission ratios for biomass burning (Andreae and Merlet, 2001). Therefore, it appears that biomass burning is a predominant contributor to atmospheric methanol over central Africa during these seasons. On the other hand, the a priori emissions employed in GEOS-Chem (Fig. 12) assume that the biogenic flux is dominant year-round. The a posteriori source reduction for this region, seen in Fig. 5, thus probably reflects an overestimate of biogenic, rather than biomass burning, emissions.

Over Brazil, biomass burning peaks in August–September (Fig. 12) and is not associated with a minimum in the observed methanol:CO slope (Fig. 11). Instead, the slope slowly increases throughout the year. This may simply reflect the seasonality of biogenic emissions, with fire emissions playing a more modest role for this region, which is broadly consistent with the a priori information (Fig. 12).

10 Impact of methanol on global photochemical production of CO and HCHO

Photochemical oxidation of methanol is a source of atmospheric HCHO and CO, two compounds that play important roles in the chemistry of OH and ozone (Logan et al., 1981; Crutzen and Zimmermann, 1991), and which serve as useful tracers for estimating anthropogenic, biogenic, and biomass burning emissions of other species (Suntharalingam et al., 2004; Warneke et al., 2007; Barkley et al., 2008; Millet et al., 2008b). Sources of HCHO and CO include primary emissions and secondary production from volatile organic compounds, including methane, isoprene, methanol, and other biogenic and anthropogenic species. In the case of CO, primary and secondary sources are thought to be of similar magnitude (Duncan et al., 2007), whereas secondary production is the predominant source of HCHO (Fortems-Cheiney et al., 2012). In both cases, identifying the key precursors is important for quantitative interpretation of the ambient concentrations. In this section, we apply a full-chemistry GEOS-Chem simulation for 2008 to quantify the global importance of methanol as a source of CO and HCHO.

Figure 13 shows the total column secondary CO production for February, April, June, August, October, and December 2008, along with the percent contribution from methanol oxidation. In the optimized simulation, methanol accounts for ~6 % of global CO and HCHO production. Methanol is an important source of CO and HCHO during spring and early summer in the Northern Hemisphere, when biogenic emissions of methanol are high but isoprene emissions are still fairly low. During April, methanol contributes up to 25 % of the secondary CO and HCHO in northern midlatitudes. During June it contributes up to ~50 % of the local CO and HCHO production in boreal regions, reflecting the later onset of the growing season at higher latitudes. Over the US Upper Midwest, we find that the maximum contribution of methanol to CO and HCHO production is ~25 %, occurring in June, which is close to the value of 20 % estimated on the basis of tower measurements by Hu et al. (2011). During other months, methanol can contribute up to 10–15 % of secondary CO and HCHO production, depending on the region. Over high isoprene emitting areas of the tropics, the fractional contribution of methanol to CO and HCHO production is modest (0–5 %). Downwind over tropical oceans, the contribution increases (10–20 %) due to methanol's longer lifetime compared to isoprene (several days versus an hour or less).

11 Summary and conclusions

We used two years of new atmospheric methanol observations from the Tropospheric Emission Spectrometer (TES) in an adjoint inversion with the GEOS-Chem CTM to quantify terrestrial emissions of methanol around the globe. A test inversion based on pseudo observations demonstrated that the TES data coverage is sufficient to accurately constrain methanol emissions on regional-to-continental scales. A posteriori uncertainties are reduced significantly compared to the a priori, and are reduced by a factor of two or more throughout most of the northern midlatitudes as well as over East Asia and parts of Central Africa and Brazil. Uncertainties are higher over Indonesia/Oceania and high latitude regions, where TES retrievals are limited.

The TES data show that current terrestrial emissions of methanol in GEOS-Chem (driven by MEGANv2.1 biogenic emissions) are too low, and that the global flux should be increased by 56 % from 76 to 117 Tg yr^{-1}. This optimized source is ~22 % of the estimated global isoprene flux (535 Tg yr^{-1}; Guenther et al., 2012), and is similar to the combined flux of all anthropogenic volatile organic compounds (estimated at 100–200 Tg yr^{-1}; Müller, 1992; Piccot et al., 1992; van Aardenne et al., 2001). We find that the largest relative increases to the a priori emissions occur over mostly semi-arid regions such as the western US, Mexico, the Iberian Peninsula, the Sahel, and central Asia. Emissions are reduced over southeastern China and over central Africa. The optimized emissions lead to a significant improvement in the methanol simulation as compared to an ensemble of aircraft measurements, though discrepancies over the western US point to missing sources in the a priori inventory (and possibly issues related to a sampling mismatch between the model and the aircraft measurements). Our optimized global terrestrial methanol flux of 117 Tg yr^{-1} also supports two other recent top-down estimates derived using in-situ (Millet et al., 2008a) and space-based (Stavrakou et al., 2011) observations (114–120 Tg yr^{-1}).

We carried out two separate sensitivity tests to assess the degree to which our derived methanol emission fluxes depend on uncertainties in model OH. An inversion that employed OH concentrations from an alternate model version led to only minor differences (< 10 %) in the a posteriori continental fluxes compared to the baseline analysis. A second sensitivity analysis that employed a parameterization to approximate OH recycling during isoprene oxidation at low NO_x indicated that uncertainties in low-NO_x isoprene chemistry most likely lead to at most a 30 % bias in our computed tropical methanol fluxes.

Since our inversion optimized the total terrestrial emission flux and did not attempt to resolve individual sources, we employed the methanol:CO correlations measured by TES to interpret the a posteriori results and improve our understanding of the underlying emission processes. These observations suggest that biogenic methanol emissions are currently underestimated over the US, western Europe, and Brazil. Over the western US, the majority of methanol emissions appear to be from sources that do not co-emit CO, suggesting high emissions from plant functional types in this region or missing sources from agriculture. An overestimate of biogenic emissions is apparent over southeastern China and central Africa during June-August, as the corresponding TES methanol:CO slopes are consistent with a predominant role for anthropogenic and biomass burning emissions, respectively.

The source optimization presented here demonstrates the importance of methanol as a photochemical precursor of CO and HCHO. Based on a full-chemistry GEOS-Chem simulation, we estimate that methanol contributes 6 % to the global secondary source of CO and HCHO, and up to ~50 % to local photochemical production of CO and HCHO in boreal regions in June, when methanol emissions are elevated but isoprene emissions are low.

Future work involving the full record of methanol observations from TES and other space-based instruments, such as the IASI sensors onboard the MetOp series of satellites and possibly CrIS on NASA's Suomi NPP satellite, should help us to better quantify methanol emissions as a function of plant functional type and phenology. These data may also prove valuable for understanding ecosystem responses to climate variability, and for distinguishing sources types for other species measured from space, such as CO_2, CO, and CH_4.

Supplementary material related to this article is available online at http://www.atmos-chem-phys-discuss.net/13/21883/2013/ acpd-13-21883-2013-supplement.pdf.

Acknowledgements. This work was supported by NASA through the Atmospheric Chemistry Modeling and Analysis Program (Grant #NNX10AG65G), the University of Minnesota Supercomputing Institute, and by the EPA Science To Achieve Results program (Grant #RD83455901). We gratefully thank John Worden and Ming Luo for their role in developing the TES methanol retrieval.

References

Andreae, M. O. and Merlet, P.: Emission of trace gases and aerosols from biomass burning, Global Biogeochem. Cy., 15, 955–966, doi:10.1029/2000GB001382, 2001.

Barkley, M. P., Palmer, P. I., Kuhn, U., Kesselmeier, J., Chance, K., Kurosu, T. P., Martin, R. V., Helmig, D., and Guenther A.: Net ecosystem fluxes of isoprene over tropical South America inferred from Global Ozone Monitoring Experiment (GOME) observations of HCHO columns, J. Geophys. Res., 113, doi:10.1029/2008JD009863, 2008.

Beer, R., Glavich, T. A., and Rider, D. M.: Tropospheric emission spectrometer for the Earth Observing System's Aura Satellite, Appl. Opt., 40, 2356–2367, 2001.

Beer, R., Shephard, M. W., Kulawik, S. S., Clough, S. A., Eldering, A., Bowman, K. W., Sander, S.P., Fisher, B. M., Payne, V. H., Luo, M., Osterman, G. B., and Worden, J. R.: First satellite observations of lower tropospheric ammonia and methanol, Geophys. Res. Lett., 35, L09801, doi:10.1029/2008GL033642, 2008.

Bousserez, N. et al.: Improved analysis error covariance matrix estimates for variational inverse problems, Q. J. Roy. Meteorol. Soc., in preparation, 2013.

Brock, C. A., Cozic, J., Bahreini, R., Froyd, K. D., Middlebrook, A. M., McComiskey, A., Brioude, J., Cooper, O. R., Stohl, A., Aikin, K. C., de Gouw, J. A., Fahey, D. W., Ferrare, R. A., Gao, R.-S., Gore, W., Holloway, J. S., Hübler, G., Jefferson, A., Lack, D. A., Lance, S., Moore, R. H., Murphy, D. M., Nenes, A., Novelli, P. C., Nowak, J. B., Ogren, J. A., Peischl, J., Pierce, R. B., Pilewskie, P., Quinn, P. K., Ryerson, T. B., Schmidt, K. S., Schwarz, J. P., Sodemann, H., Spackman, J. R., Stark, H., Thomson, D. S., Thornberry, T., Veres, P., Watts, L. A., Warneke, C., and Wollny, A. G.: Characteristics, sources, and transport of aerosols measured in spring 2008 during the aerosol, radiation, and cloud processes affecting Arctic Climate (ARCPAC) Project, Atmos. Chem. Phys., 11, 2423–2453, doi:10.5194/acp-11-2423-2011, 2011.

Byrd, R. H., Lu, P. H., Nocedal, J., and Zhu, C. Y.: A limited memory algorithm for bound constrained optimization, Sci. Comput., 16, doi:10.1137/0916069, 1995.

Cady-Pereira, K. E., Shephard, M. W., Millet, D. B., Luo, M., Wells, K. C., Xiao, Y. Payne, V. H., Worden, J.: Methanol from TES global observations: retrieval algorithm and seasonal and spatial variability, Atmos. Chem. Phys., 12, 8189–8203, doi:10.5194/acp-12-8189-2012, 2012.

Carpenter, L. J., Lewis, A. C., Hopkins, J. R., Read, K. A., Longley, I. D., Gallagher, M. W.: Uptake of methanol to the North Atlantic Ocean surface, Global Biogeochem. Cy., 18, GB4027, doi:10.1029/2004GB002294, 2004.

Choi, W., Faloona, I. C., Bouvier-Brown, N. C., McKay, M., Goldstein, A. H., Mao, J., Brune, W. H., LaFranchi, B. W., Cohen, R. C., Wolfe, G. M., Thornton, J. A., Sonnenfroh, D. M., and Millet, D. B.: Observations of elevated formaldehyde over a forest canopy suggest missing sources from rapid oxidation of arboreal hydrocarbons, Atmos. Chem. Phys., 10, 8761–8781, doi:10.5194/acp-10-8761-2010, 2010.

Crutzen, P. J. and Zimmermann, P. H.: The changing photochemistry of the troposphere, Tellus A, 43, 136–151, 1991.

de Gouw, J. A., Middlebrook, A. M., Warneke, C., Goldan, P. D., Kuster, W. C., Roberts, J. M., Fehsenfeld, F. C., Worsnop, D. R., Canagaratna, M. R., Pszenny, A. A. P., Keene, W. C., Marchewka, M., Bertman, S. B., and Bates, T. S.: Budget of organic carbon in a polluted atmosphere: results from the New England Air Quality Study in 2002, J. Geophys. Res., 110, D16305, doi:10.1029/2004JD005623, 2005.

Duncan, B. N., Logan, J. A., Bey, I., Megretskaia, I. A., Yantosca, R. M., Novelli, P. C., Jones, N. B., Rinsland, C. P.: Global budget of CO, 1988–1997: source estimates and validation with a global model, J. Geophys. Res., 112, D22301, doi:10.1029/2007JD008459, 2007.

Fall, R.: Abundant oxygenates in the atmosphere: A biochemical perspective, Chem. Rev., 103, 4941–4951, doi:10.1021/cr0206521, 2003.

Fall, R. and Benson, A. A.: Leaf methanol –The simplest natural product from plants, Trends Plant Sci., 1, 296–301, doi:10.1016/1360-1385(96)88175-1, 1996.

Fehsenfeld, F. C., Ancellet, G., Bates, T. S., Goldstein, A. H., Hardesty, R. M., Honrath, R., Law, K. S., Lewis, A. C., Leaitch, R., McKeen, S., Meagher, J., Parrish, D. D., Pszenny, A. A. P., Russell, P. B., Schlager, H., Seinfeld, J., Talbot, R., and Zbinden, R.: International Consortium for Atmospheric Research on Transport and Transformation (ICARTT): North America to Europe – Overview of the 2004 summer field study, J. Geophys. Res., 111, D23S01, doi:10.1029/2006JD007829, 2006.

Fortems-Cheiney, A., Chevallier, F., Pison, I., Bousquet, P., Saunois, M., Szopa, S., Cressot, C., Kurosu, T. P., Chance, K., and Fried, A.: The formaldehyde budget as seen by a global-scale multi-constraint and multi-species inversion system, Atmos. Chem. Phys., 12, 6699–6721, doi:10.5194/acp-12-6699-2012, 2012.

Galbally, I. E. and Kirstine, W.: The production of methanol by flowering plants and the global cycle of methanol, J. Atmos. Chem., 43, 195-229, 2002.

Goldan, P. D., Trainer, M., Kuster, W. C., Parrish, D. D., Carpenter, J., Roberts, J. M., Yee, J. E., Fehsenfeld, F. C.: Measurements of hydrocarbons, oxygenated hydrocarbons, carbon monoxide, and nitrogen oxides in an urban basin in Colorado: implications for emission inventories, J. Geophys. Res., 100, 22771–22783, 1995.

Guenther, A. B., Jiang, X., Heald, C. L., Sakulyanontvittaya, T., Duhl, T., Emmons, L. K., and Wang, X.: The Model of Emissions of Gases and Aerosols from Nature version 2.1 (MEGAN2.1): an extended and updated framework for modeling biogenic emissions, Geosci. Model Dev., 5, 1471–1492, doi:10.5194/gmd-5-1471-2012, 2012.

Hansen, P. C.: Rank-Deficient and Discrete Ill-Posed Problems: Numerical Aspects of Linear Inversion, SIAM, Philadelphia, USA, 1998.

Heikes, B. G., Chang, W. N., Pilson, M. E. Q., Swift, E., Singh, H. B, Guenther, A., Jacob, D. J., Field, B. D., Fall, R., Riemer, D., and Brand, L.: Atmospheric methanol budget and ocean implication, Global Biogeochem. Cy., 16, 1133, doi:10.1029/2002GB001895, 2002.

Henze, D. K., Seinfeld, J. H., and Shindell, D. T.: Inverse modeling and mapping US air quality influences of inorganic PM2.5 precursor emissions using the adjoint of GEOS-Chem, Atmos. Chem. Phys., 9, 5877–5903, doi:10.5194/acp-9-5877-2009, 2009.

Holzinger, R., Warneke, C., Hansel, A., Jordan, A., Lindinger, W., Scharffe, D. H., Schade, G., Crutzen, P. J.: Biomass burning as a source of formaldehyde, acetaldehyde, methanol, acetone, acetonitrile, and hydrogen cyanide, Geophys. Res. Lett., 26, 1161–1164, 1999.

Howard, C. J., Kumar, A., Malkina, I., Mitloehner, F., Green, P.G., Flocchini, R. G., and Kleeman, M. J.: Reactive organic gas emissions from livestock feed contribute significantly to ozone production in Central California, Envir. Sci. Tech., 44, 2309–2314, doi:10.1021/es902864u, 2010.

Hu, L., Millet, D. B., Mohr, M. J., Wells, K. C., Griffis, T. J., and Helmig, D.: Sources and seasonality of atmospheric methanol based on tall tower measurements in the US Upper Midwest, Atmos. Chem. Phys., 11, 11145–11156, doi:10.5194/acp-11-11145-2011, 2011.

Jacob, D. J., Crawford, J. H., Maring, H., Clarke, A. D., Dibb, J. E., Emmons, L. K., Ferrare, R. A., Hostetler, C. A., Russell, P. B., Singh, H. B., Thompson, A. M., Shaw, G. E., McCauley, E., Pederson, J. R., Fisher, J. A.: The Arctic Research of the Composition of the Troposphere from Aircraft and Satellites (ARCTAS) mission: design, execution, and first results, Atmos. Chem. Phys., 10, 5191–5212, doi:10.5194/acp-10-5191-2010, 2010.

Jiang, Z., Jones, D. B. A., Kopacz, M., Liu, J., Henze, D. K., and Heald, C.: Quantifying the impact of model errors on top-down estimates of carbon monoxide emissions using satellite observations, J. Geophys. Res., 116, D15306, doi:10.1029/2010JD015282, 2011.

Jiang, Z., Jones, D. B. A., Worden, H. M., Deeter, M. N., Henze, D. K., Worden, J., and Bowman, K. W., Brenninkmeijer, C. A. M., Schuck, T. J.: Impact of model errors in convective transport on CO source estimates inferred from MOPITT CO retrievals, J. Geophys. Res., 118, 2073–2083, doi:10.1002/jgrd.50216, 2013.

Johnson, M. T.: A numerical scheme to calculate temperature and salinity dependent air-water transfer velocities for any gas, Ocean Sci., 6, 913–932, doi:10.5194/os-6-913-2010, 2010.

Karl, T., Harley, P., Emmons, L., Thornton, B., Guenther, A., Basu, C., Turnipseed, A., and Jardine, K.: Efficient atmospheric cleansing of oxidized organic trace gases by vegetation, Science, 330, 816–819, doi:10.1126/science.1192534, 2010.

Kopacz, M., Jacob, D. J., Fisher, J. A., Logan, J. A., Zhang, L., Megretskaia, I. A., Yantosca, R. M., Singh, K., Henze, D. K., Burrows, J. P., Buchwitz, M., Khlystova, I., McMillan, W. W., Gille, J. C., Edwards, D. P., Eldering, A., Thouret, V., and Nedelec, P.: Global estimates of CO sources with high resolution by adjoint inversion of multiple satellite datasets (MOPITT, AIRS, SCIAMACHY, TES), Atmos. Chem. Phys., 10, 855–876, doi:10.5194/acp-10-855-2010, 2010.

Kopacz, M., Jacob, D. J., Henze, D. K., Heald, C. L., Streets, D. G., and Zhang, Q.: Comparison of adjoint and analytical Bayesian inversion methods for constraining Asian sources of carbon monoxide using satellite (MOPITT) measurements of CO columns, J. Geophys. Res., 114, D04305, doi:10.1029/2007JD009264, 2009.

Kopacz, M., Mauzerall, Wang, J., Leibensperger, E. M., Henze, D. K., and Singh, K.: Origin and radiative forcing of black carbon transported to the Himalayas and Tibetan Plateau, Atmos. Chem. Phys., 11, 2837–2852, doi:10.5194/acp-11-2837-2011, 2011.

Kubistin, D., Harder, H., Martinez, M., Rudolf, M., Sander, R., Bozem, H., Eerdekens, G., Fischer, H., Gurk, C., Klüpfel, T., Königstedt, R., Parchatka, U., Schiller, C. L., Stickler, A., Taraborrelli, D., Williams, J., and Lelieveld, J.: Hydroxyl radicals in the tropical troposphere over the Suriname rainforest: comparison of measurements with the box model MECCA, Atmos. Chem. Phys., 10, 9705-9728, doi:10.5194/acp-10-9705-2010, 2010.

Lelieveld, J., Butler, T. M., Crowley, J. N., Dillon, T. J., Fischer, H., Ganzeveld, L., Harder, H., Lawrence, M.G., Martinez, M., Taraborrelli, D., and Williams, J.: Atmospheric oxidation capacity sustained by a tropical forest, Nature, 452, 737–740, doi:10.1038/nature06870, 2008.

Lewis, A. C., Hopkins, J. R., Carpenter, L. J., Stanton, J., Read, K. A., and Pilling, M. J.: Sources and sinks of acetone, methanol, and acetaldehyde in North Atlantic marine air, Atmos. Chem. Phys., 5, 1963–1974, doi:10.5194/acp-5-1963-2005, 2005.

Logan, J. A., Prather, M. J., Wofsy, S. C., and McElroy, M. B.: Tropospheric chemistry – A global perspective, J. Geophys. Res., 86, 7210–7254, 1981.

Malkina, I. L., Kumar, A., Green, P. G., and Mitloehner, F. M.: Identification and quantitation of volatile organic compounds emitted from dairy silages and other feedstuffs, J. Environ. Qual., 40, 28–36, doi:10.2134/jeq2010.0302, 2011.

Mao, J., Ren, X., Zhang, L., Van Duin, D. M., Cohen, R. C., Park, J.-H., Goldstein, A. H., Paulot, F., Beaver, M. R., Crounse, J. D., Wennberg, P. D., DiGangi, J. P., Henry, S. B., Keutsch, F. N., Park, C., Schade, G. W., Wolfe, G. M., Thornton, J. A., and Brune, W. H.: Insights into hydroxyl measurements and atmospheric oxidation in a California forest, Atmos. Chem. Phys., 12, 8009–8020, doi:10.5194/acp-12-8009-2012, 2012.

Millet, D. B., Donahue, N. M., Pandis, S. N., Polidori, A., Stanier, C. O., Turpin, B. J., and Goldstein, A. H.: Atmospheric volatile organic compound measurements during the Pittsburgh Air Quality Study: Results, interpretation, and quantification of primary and secondary contributions, J. Geophys. Res., 110, D07S07, doi:10.1029/2004JD004601, 2005.

Millet, D. B., Jacob, D. J., Turquety, S., Hudman, R. C., Wu, S., Fried, A., Walega, J., Heikes, B. G., Blake, D. R., Singh, H. B., Anderson, B. E., and Clarke, A. D.: Formaldehyde distribution over North America: implications for satellite retrievals of formaldehyde columns and isoprene emission, J. Geophys. Res., 111, D24S02, doi:10.1029/2005JD006853, 2006.

Millet, D. B., Jacob, D. J., Custer, T. G., de Gouw, J. A., Goldstein, A. H., Karl, T., Singh, H. B., Sive, B. C., Talbot, R. W., Warneke, C., and Williams, J.: New constraints on terrestrial and oceanic sources of atmospheric methanol, Atmos. Chem. Phys., 8, 6887–6905, doi:10.5194/acp-8-6887-2008, 2008a.

Millet, D. B., Jacob, D. J., Boersma, K. F., Fu, T. M., Kurosu, T. P., Chance, K., Heald, C. L., and Guenther, A., Spatial distribution of isoprene emissions from North America derived from formaldehyde column measurements by the OMI satellite sensor, J. Geophys. Res., 113, D02307, doi:10.1029/2007JD008950, 2008b.

Millet, D. B., Apel, E., Henze, D. K., Hill, J., Marshall, J. D., Singh, H. B., and Tessum, C. W.: Natural and anthropogenic ethanol sources in North America and potential atmospheric impacts of ethanol fuel use, Environ. Sci. Tech., 46, 8484–8492, doi:10.1021/es300162u, 2012.

Müller, J. F.: Geographical distribution and seasonal variation of surface emissions and deposition velocities of atmospheric trace gases, J. Geophys. Res., 97, 3787–3804, 1992.

Nightingale, P. D., Malin, G., Law, C. S., Watson, A. J., Liss, P. S., Liddicoat, M. I., Boutin, J., and Upstill-Goddard, R. C.: In situ evaluation of air-sea gas exchange parameterizations using novel conservative and volatile tracers, Global Biogeochem. Cy., 14, 373–387, doi:10.1029/1999GB900091, 2000.

Parrington, M., Palmer, P. I., Henze, D. K., Tarasick, D. W., Hyer, E. J., Owen, R. C., Helmig, D., Clerbaux, C., Bowman, K. W., Deeter, M. N., Barratt, E. M., Coheur, P.-F., Hurtmans, D., Jiang, Z., George, M., and Worden, J. R.: The influence of boreal biomass burning emissions on the distribution of tropospheric ozone over North America and the North Atlantic during 2010, Atmos. Chem. Phys., 12, 2077–2098, doi:10.5194/acp-12-2077-2012, 2012.

Parrish, D. D., Allen, D. T., Bates, T. S., Estes, M., Fehsenfeld, F. C., Feingold, G., Ferrare, R., Hardesty, R. M., Meagher, J. F., Nielsen-Gammon, J. W., Pierce, R. B., Ryerson, T. B., Seinfeld, J. H., Williams, E. J.: Overview of the Second Texas Air Quality Study (TexAQS II) and the Gulf of Mexico Atmospheric Composition and Climate Study (GoMACCS), J. Geophys. Res., 114, D00F13, doi:10.1029/2009JD011842, 2009.

Parrish, D. D., Kondo, Y., Cooper, O. R., Brock, C. A., Jaffe, D. A., Trainer, M., Ogawa, T., Hubler, G., and Fehsenfeld, F. C.: Intercontinental Transport and Chemical Transformation 2002 (ITCT 2K2) and Pacific Exploration of Asian Continental Emission (PEACE) experiments: An overview of the 2002 winter and spring intensives, J. Geophys. Res., 109, D23S01, doi:10.1029/2004JD004980, 2004.

Piccot, S. D., Watson, J. J., and Jones, J. W.: A global inventory of volatile organic compound emissions from anthropogenic sources, J. Geophys. Res., 97, 9897–9912, 1992.

Pugh, T. A. M., MacKenzie, A. R., Hewitt, C. N., Langford, B., Edwards, P. M., Furneaux, K. L., Heard, D. E., Hopkins, J. R., Jones, C. E., Karunaharan, A., Lee, J., Mills, G., Misztal, P., Moller, S., Monks, P. S., and Whalley, L. K.: Simulating atmospheric composition over a South-East Asian tropical rainforest: performance of a chemistry box model, Atmos. Chem. Phys., 10, 279–298, doi:10.5194/acp-10-279-2010, 2010.

Rodgers, C. D.: Inverse Methods for Atmospheric Sounding: Theory and Practice, World Scientific, Tokyo, 2000.

Shephard, M. W., Cady-Pereira, K. E., Luo, M., Henze, D. K., Pinder, R. W., Walker, J. T., Rinsland, C. P., Bash, J. O., Zhu, L., Payne, V. H., and Clarisse, L.: TES ammonia retrieval strategy and global observations of the spatial and seasonal variability of ammonia, Atmos. Chem. Phys., 11, 10743–10763, doi:10.5194/acp-11-10743-2011, 2011.

Singh, H. B, Kanakidou, M., Crutzen, P. J., and Jacob, D. J.: High concentrations and photochemical fate of oxygenated hydrocarbons in the global troposphere, Nature, 378, 50–54, 1995.

Singh, H. B, Chen, Y., Staudt, A., Jacob, D., Blake, D., Heikes, B., and Snow, J.: Evidence from the Pacific troposphere for large global sources of oxygenated organic compounds, Nature, 410, 1078–1081, 2001.

Singh, H. B., Brune, W. H., Crawford, J. H., Flocke, F., and Jacob, D. J.: Chemistry and transport of pollution over the Gulf of Mexico and the Pacific: spring 2006 INTEX-B campaign overview and first results, Atmos. Chem. Phys., 9, 2301–2318, doi:10.5194/acp-9-2301-2009, 2009.

Singh, K., Jardak, M., Sandu, A., Bowman, K., Lee, M., and Jones, D.: Construction of non-diagonal background error covariance matrices for global chemical data assimilation, Geosci. Model Dev. 4, 299–316, doi:10.5194/gmd-4-299-2011, 2011.

Stavrakou, T., Guenther, A., Razavi, A., Clarisse, L., Clerbaux, C., Coheur, P.F., Hurtmans, D., Karagulian, F., De Maziere, M., Vigouroux, C., Amelynck, C., Schoon, N., Laffineur, Q., Heinesch, B., Aubinet, M., Rinsland, C., and Muller, J. F.: First space-based derivation of the global atmospheric methanol emission fluxes, Atmos. Chem. Phys., 11, 4873–4898, doi:10.5194/acp-11-4873-2011, 2011.

Stone, D., Evans, M. J., Edwards, P. M., Commane, R., Ingham, T., Rickard, A. R., Brookes, D. M., Hopkins, J., Leigh, R. J., Lewis, A. C., Monks, P. S., Oram, D., Reeves, C. E., Stewart, D., and Heard, D. E.: Isoprene oxidation mechanisms: measurements and modelling of OH and HO_2 over a South-East Asian tropical rainforest during the OP3 field campaign, Atmos. Chem. Phys., 11, 6749–6771, doi:10.5194/acp-11-6749-2011, 2011.

Suntharalingam, P., Jacob, D. J., Palmer, P. I., Logan, J. A., Yantosca, R. M., Xiao, Y. P., Evans, M. J., Streets, D. G., Vay, S. L., and Sachse, G. W.: Improved quantification of Chinese carbon fluxes using CO_2/CO correlations in Asian outflow, J. Geophys. Res., 109, D18S18, doi:10.1029/2003JD004362, 2004.

Tie, X., Guenther, A., and Holland, E.: Biogenic methanol and its impacts on tropospheric oxidants, Geophys. Res. Lett., 30, 1881, doi:10.1029/2003GL017167, 2003.

Tyndall, G. S., Cox, R. A., Granier, C., Lesclaux, R., Moortgat, G. K., Pilling, M. J., Ravishankara, A. R., and Wallington, T. J.: Atmospheric chemistry of small organic peroxy radicals, J. Geophys. Res., 106, 12157–12182, 2001.

van Aardenne, J. A., Dentener, F. J., Olivier, J. G. J., Goldewijk, C., and Lelieveld, J.: A 1 degrees x 1 degrees resolution data set of historical anthropogenic trace gas emissions for the period 1890–1990, Global Biogeochem. Cy., 15, 909–928, doi:10.1029/2000GB001265, 2001.

van der Werf, G. R., Randerson, J. T., Giglio, L., Collatz, G. J., Mu, M., Kasibhatla, P. S., Morton, D. C., DeFries, R. S., Jin, Y., and van Leeuwen, T. T.: Global fire emissions and the contribution of deforestation, savanna, forest, agricultural, and peat fires (1997–2009), Atmos. Chem. Phys., 10, 11707–11735, doi:10.5194/acp-10-11707-2010, 2010.

Wang, J., Xu, X., Henze, D. K., Zeng, J., Ji, Q., Tsay, S.-C., and Huang, J.: Top-down estimate of dust emissions through integration of MODIS and MISR aerosol retrievals with the GEOS-Chem adjoint model, Geophys. Res. Lett., 39, L08802, doi:10.1029/2012GL051136, 2012.

Warneke, C., de Gouw, J. A., Holloway, J. S., Peischl, J., Ryerson, T. B., Atlas, E. L., and Blake, D. R.: Airborne measurements of volatile organic compounds in the Los Angeles Basin and the Central Valley, Abstract A12A-01 presented at 2010 Fall Meeting, AGU, San Francisco, CA, 13–17 December, 2010.

Warneke, C., McKeen, S. A., de Gouw, J. A., Goldan, P. D., Kuster, W. C., Holloway, J. S., Williams, E. J., Lerner, B. M., Parrish, D. D., Trainer, M., Fehsenfeld, F. C., Kato, S., Atlas, E. L., Baker, A., and Blake, D.R.: Determination of urban volatile organic compound emission ratios and comparison with an emissions database, J. Geophys. Res., 112, D10S47, doi:10.1029/2006JD007930, 2007.

Wells, K. C., Millet, D. B., Hu, L., Cady-Pereira, K. E., Xiao, Y., Shephard, M. W., Clerbaux, C. L., Clarisse, L., Coheur, P.-F., Apel, E. C., de Gouw, J., Warneke, C., Singh, H. B., Goldstein, A. H., and Sive, B. C.: Tropospheric methanol observations from space: retrieval evaluation and constraints on the seasonality of biogenic emissions, Atmos. Chem. Phys., 12, 5897–5912, doi:10.5194/acp-12-5897-2012, 2012.

Williams, J., Holzinger, R., Gros, V., Xu, X., Atlas, E., and Wallace, D. W. R.: Measurements of organic species in air and seawater from the tropical Atlantic, Geophys. Res. Lett., 31, L23S06, doi:10.1029/2004GL020012, 2004.

Yang, W., Shabanov, N. V., Huang, D., Wang, W., Dickinson, R. E., Nemani, R. R., Knyazikhin, Y., Myneni, R. B.: Analysis of leaf area index products from combination of MODIS Terra and Aqua data, Remote Sens. Environ., 104, 297–312, 2006.

Zhang, L., Jacob, D. J., Kopacz, M., Henze, D. K., Singh, K., and Jaffe, D. A.: Intercontinental source attribution of ozone pollution at western US sites using an adjoint method, Geophys. Res. Lett., 36, doi:10.1029/2009GL037950, 2009.

Zhu, C., Byrd, R. H., Lu, P., and Nocedal, J.: L-BFGS-B: a limited memory FORTRAN code for solving bound constrained optimization problems, Tech. rep., Northwestern University, 1994.

Zhu, L., Henze, D. K., Cady-Pereira, K. E., Shephard, M. W., Luo, M., Pinder, R. W., Bash, J. O., and Jeong, G.-R.: Constraining U.S. ammonia emissions using TES remote sensing observations and the GEOS-Chem adjoint model, J. Geophys. Res. Atmos., 118, 3355–3368, doi:10.1002/jgrd.50166, 2013.

Table 1. Pseudo observation analysis[a].

Region[b]	Derived:actual emissions
North America	0.90, 1.04
South America	0.93, 1.06
Central/Southern Africa	0.96, 1.00
Europe	1.02, 0.99
Southeast Asia/India	0.96, 1.01
Siberia	0.87, 1.14
Indonesia/Oceania	0.78, 1.22

[a] A posteriori annual terrestrial emissions are shown normalized to the actual emissions prescribed for the test inversion. The two numbers listed correspond to separate tests in which the a priori emissions were decreased (0.5×) and increased (1.5×), respectively, relative to the actual values.

[b] Regions are as outlined in Fig. S3.

Title Page
Abstract | Introduction
Conclusions | References
Tables | Figures
◂◂ | ▸▸
◂ | ▸
Back | Close
Full Screen / Esc
Printer-friendly Version
Interactive Discussion

Table 2. Optimization of terrestrial methanol emissions based on the TES measurements.

Region[a]	A priori (Tg yr^{-1})	A posteriori (Tg yr^{-1})[b]	Alt OH (Tg yr^{-1})[c]	p3OH (Tg yr^{-1})[d]	γtests (Tg yr^{-1})[e]
North America	8.0	18.0	18.8	–	17.3, 18.0, 19.3
South America	16.0	19.1	18.2	–	19.0, 19.0, 19.5
Central/Southern Africa	22.5	27.1	26.0	–	26.8, 27.2, 27.3
Europe	5.1	13.9	14.1	–	13.5, 14.1, 13.9
Southeast Asia/India	14.0	26.7	27.5	–	26.2, 27.0, 27.4
Siberia	3.5	4.7	5.0	–	4.8, 4.8, 4.8
Indonesia/Oceania	6.0	7.6	7.5	–	7.5, 7.5, 7.9
Brazil	5.7	6.4	6.1	8.2	6.4, 6.4, 6.5
Central Africa	8.4	6.2	5.6	7.8	6.3, 6.2, 5.9

[a] Regions are as outlined in Fig. S3.

[b] Baseline inversion using standard model chemistry.

[c] Test inversion using alternate global OH fields (see text).

[d] *p*3OH is a parameterization that approximates the effects of OH recycling in high-isoprene, low-NO_x environments (see text).

[e] Sensitivity tests of the a priori constraint. The three numbers listed correspond to γ-values of 1.0, 0.01, and 0, respectively.

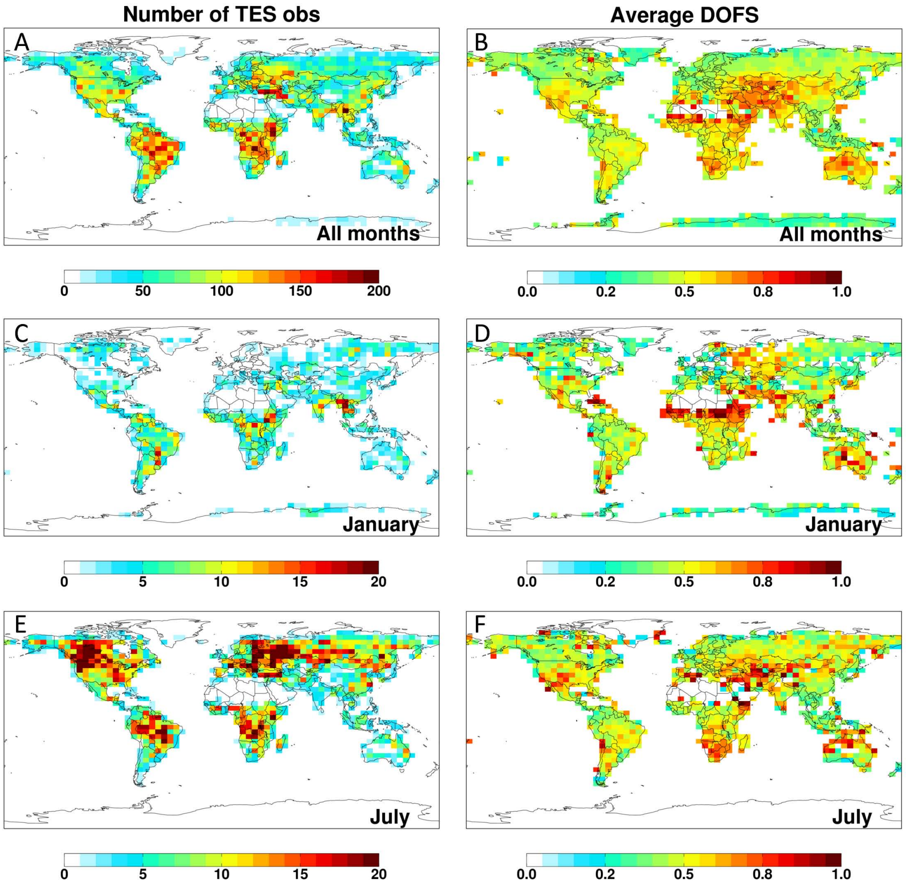

Fig. 1. TES sampling frequency and degrees of freedom for signal (DOFS) for methanol. Shown is the number of TES methanol observations in each 4° × 5° GEOS-Chem grid box, and the average DOFS for those observations, during: **(A)–(B)** all months of 2008–2009; **(C)–(D)** January 2008 and 2009; and **(E)–(F)** July 2008 and 2009.

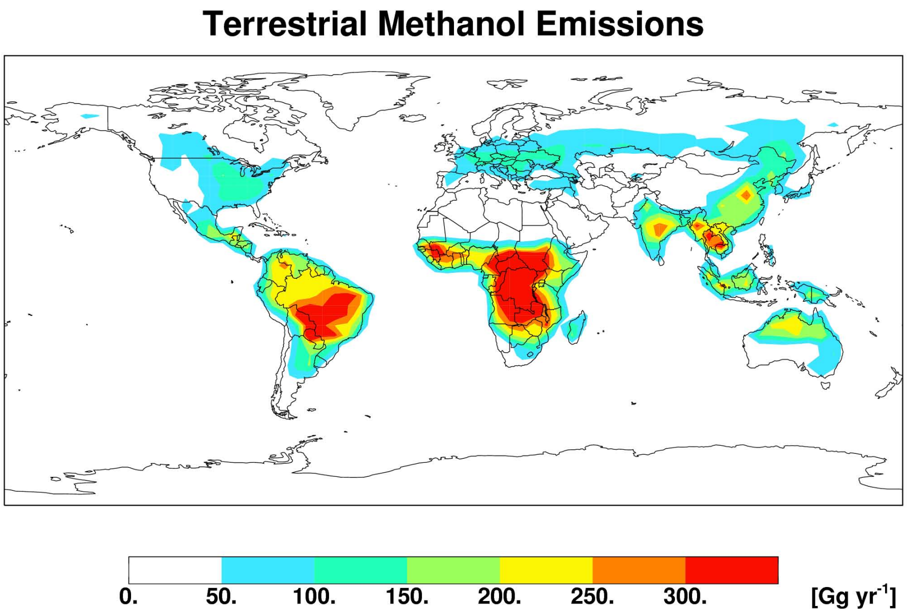

Fig. 2. Annual terrestrial emissions (Gg yr^{-1}) of methanol in the GEOS-Chem a priori simulation (year 2008) from anthropogenic activities, biomass burning, biofuel burning, and terrestrial biota.

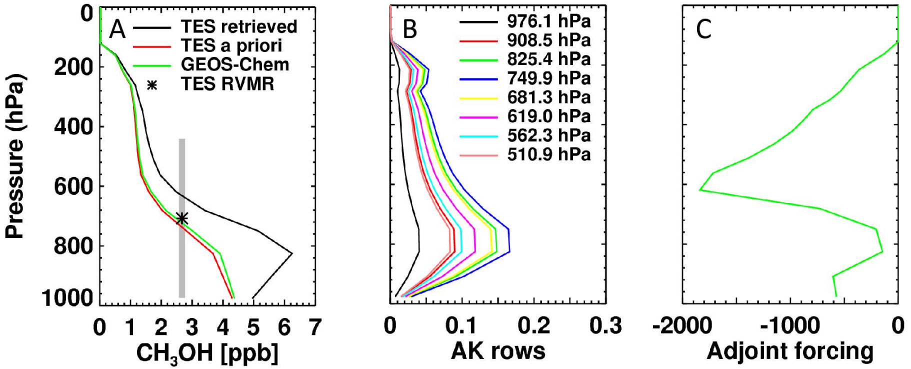

Fig. 3. Example TES methanol retrieval and corresponding adjoint forcing. **(A)** Retrieved methanol profile (black line), with the a priori profile (red line), the GEOS-Chem model profile with the TES a priori and averaging kernel applied (green line), and the TES representative volume mixing ratio (RVMR, black symbol). The shaded bar indicates the vertical range over which the RVMR applies, corresponding to the full width at half-maximum of the averaging kernel peak. **(B)** Rows of the averaging kernel for this retrieval, which has 0.78 degrees of freedom for signal (DOFS). **(C)** The corresponding adjoint forcing ($dJ/d\boldsymbol{p}$) for this example.

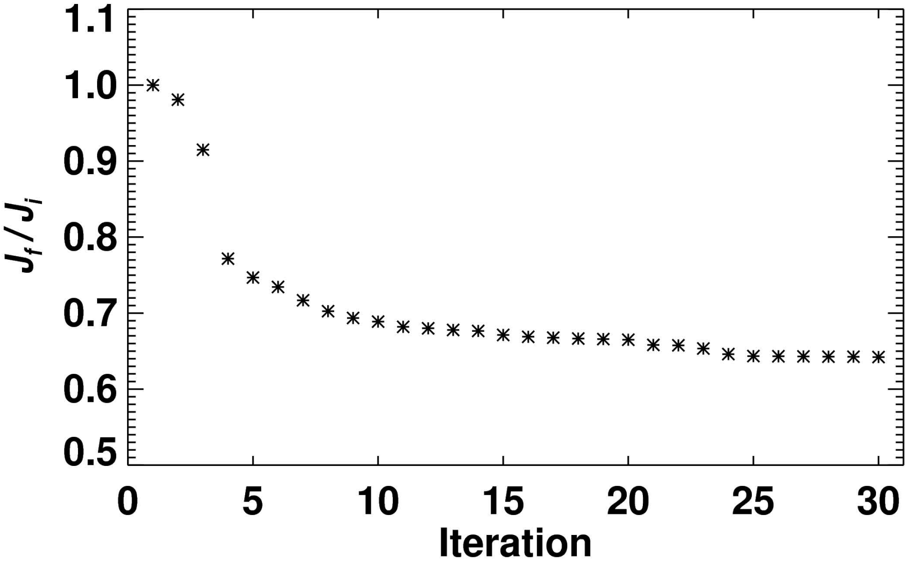

Fig. 4. Cost function evolution for the adjoint optimization using TES observations, plotted as the ratio of the final (J_f) to initial (J_i) value for each iteration.

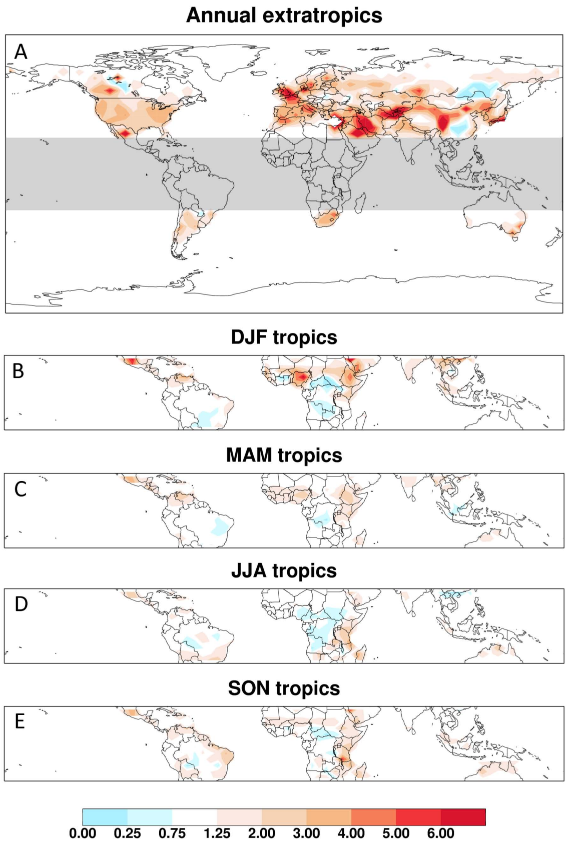

Fig. 5. Scale factors for the a priori terrestrial methanol emissions optimized on the basis of the TES observations. **(A)** Annual scale factors for the extratropics. **(B)–(D)** Seasonal scale factors for the tropics (DJF = December, January February; MAM March, April, May; JJA = June, July, August; SON = September, October, November).

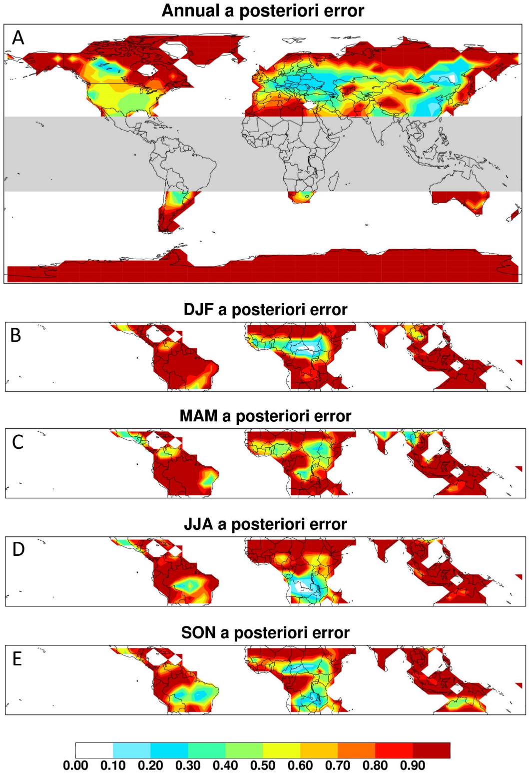

Fig. 6. A posteriori error estimate for the optimized methanol emissions (a priori error = 1.0, i.e., 100 %). **(A)** Annual a posteriori error for the extratropics. **(B–D)** Seasonal a posteriori error for the tropics (DJF = December, January February; MAM = March, April, May; JJA = June, July, August; SON = September, October, November).

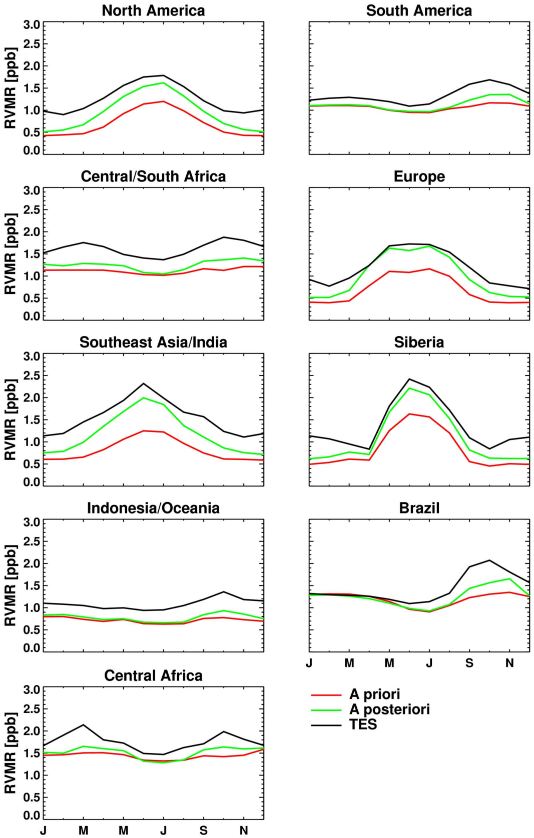

Fig. 7. Timelines of monthly-averaged representative volume mixing ratio (RVMR) as measured by TES (black) and simulated by GEOS-Chem, averaged over the regions in Fig. S3. The red line is the a priori GEOS-Chem simulation, and the green line is the a posteriori simulation with optimized terrestrial sources.

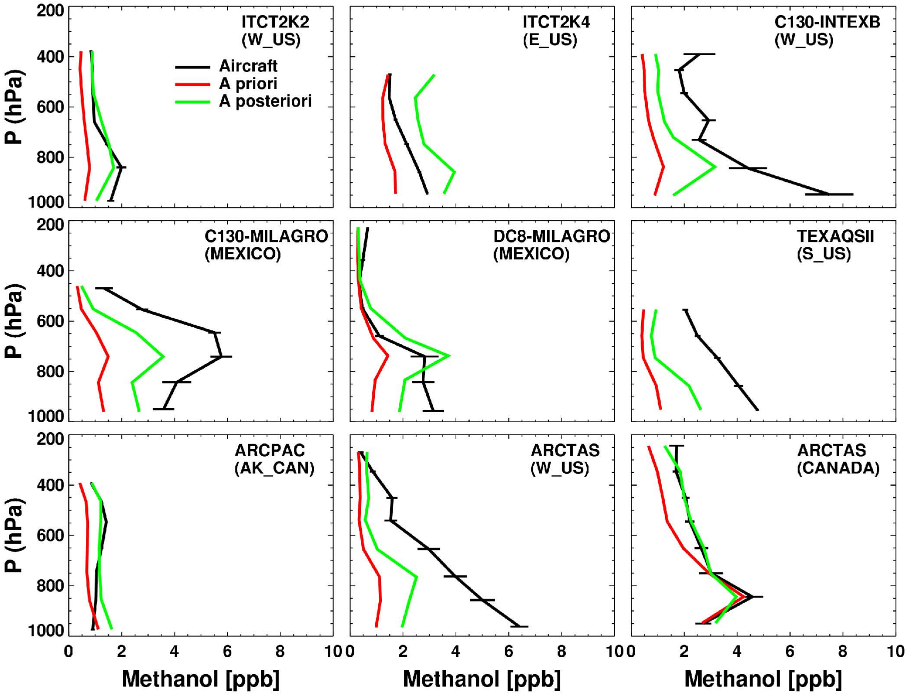

Fig. 8. Vertical profiles of methanol concentrations over North America. Each profile represents a campaign average over the region specified in the panel. Aircraft measurements are shown in black with the ±95 % confidence limits for each vertical bin indicated by the horizontal bars. The red line is the a priori GEOS-Chem simulation, and the green line is the GEOS-Chem simulation after a posteriori scaling factors have been applied.

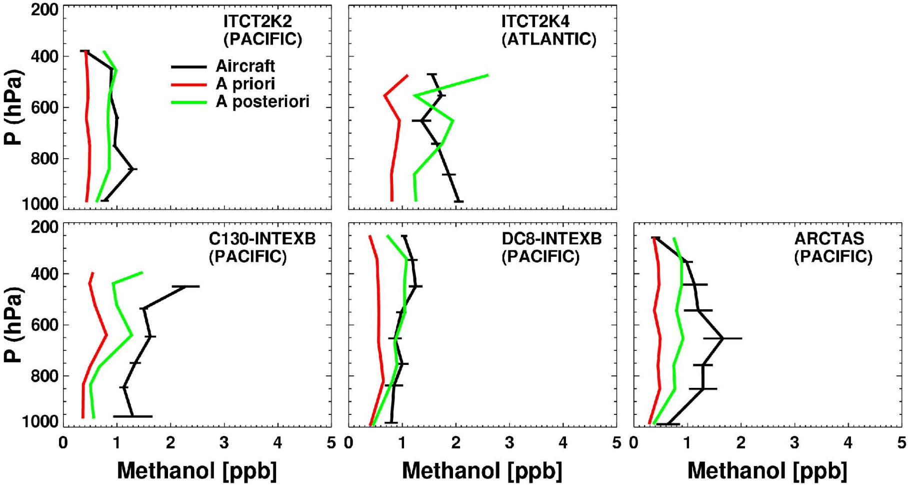

Fig. 9. Vertical profiles of methanol concentrations over ocean. Each profile represents a campaign average over the region specified in the panel. Aircraft measurements are shown in black with the ± 95 % confidence limits for each vertical bin indicated by the horizontal bars. The red line is the a priori GEOS-Chem simulation, and the green line is the GEOS-Chem simulation after a posteriori scaling factors have been applied.

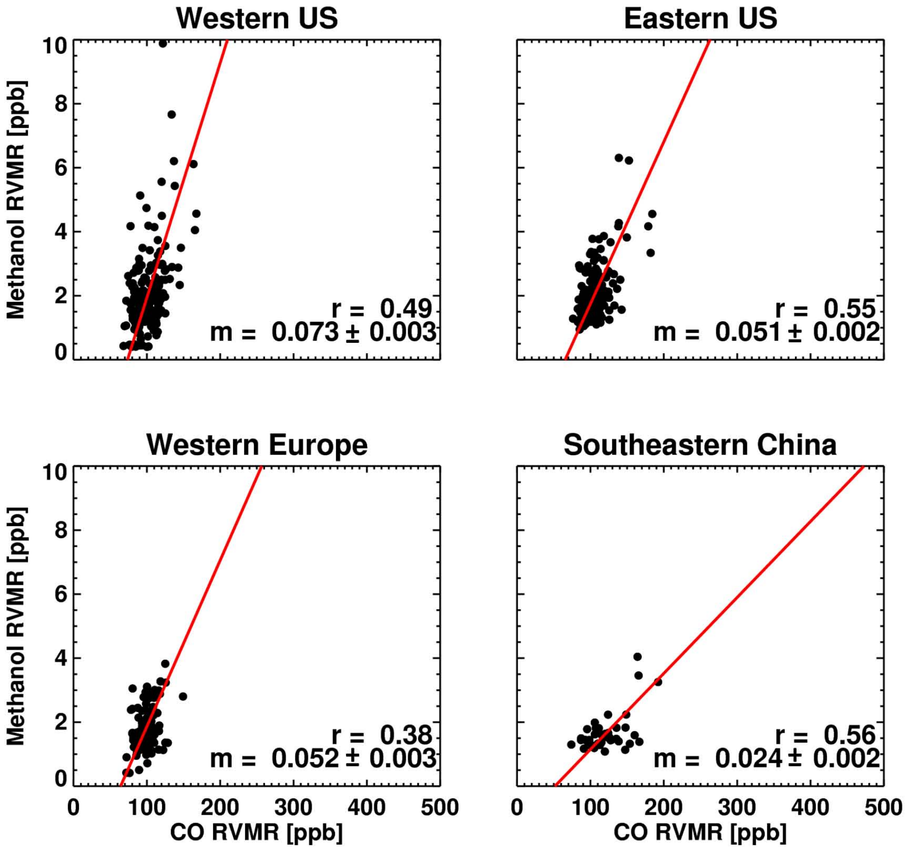

Fig. 10. Extratropical methanol:CO correlations as measured by TES during June-August. Regions are as outlined in Fig. S3. The TES CO RVMR is calculated by applying the TES methanol RVMR weighting function to the retrieved CO profile. Slopes are calculated using reduced major axis regression.

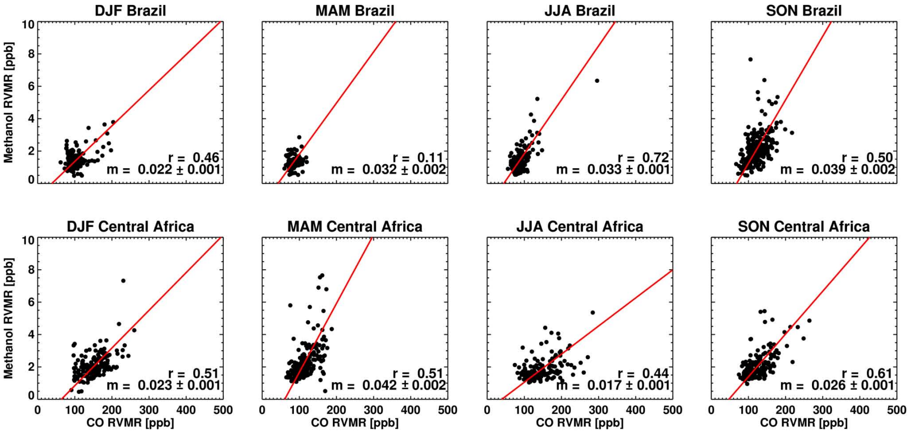

Fig. 11. Tropical methanol:CO correlations as measured by TES. Regions are as outlined in Fig. S3. The TES CO RVMR is calculated by applying the TES methanol RVMR weighting function to the retrieved CO profile. Slopes are calculated using reduced major axis regression.

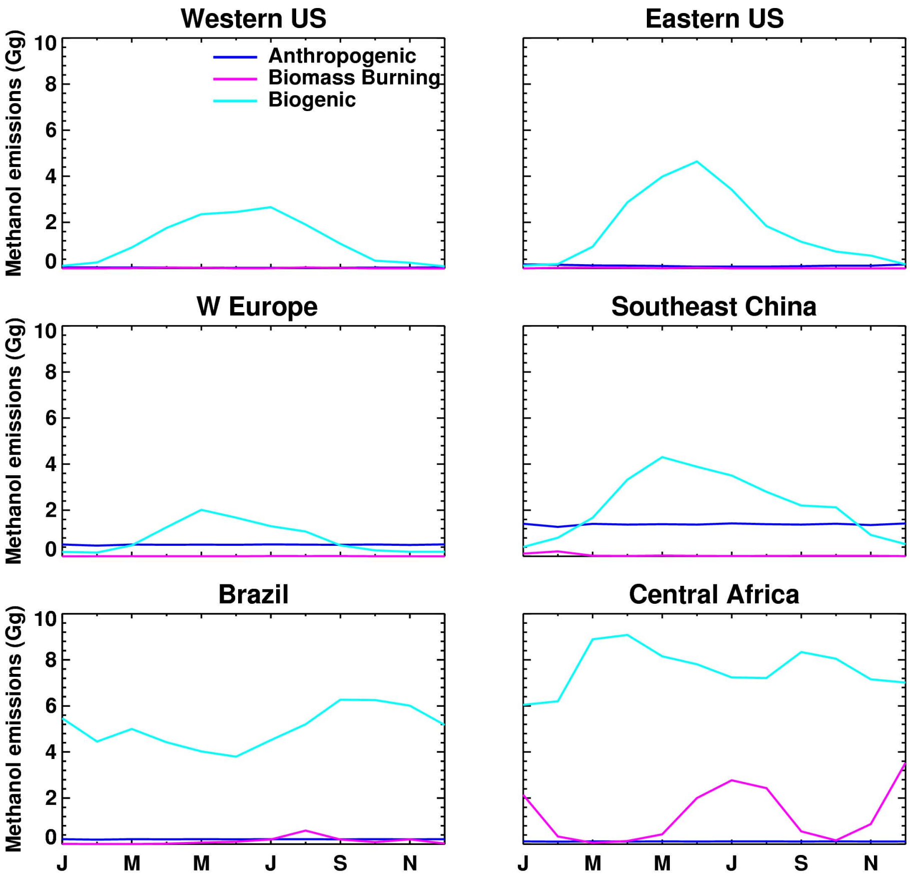

Fig. 12. Seasonality of methanol emissions from anthropogenic (blue), biomass burning (pink), and biogenic sources (cyan) in the GEOS-Chem a priori simulation for the regions in Fig. S3.

Title Page
Abstract | Introduction
Conclusions | References
Tables | Figures
◀| |▶
◀ ▶
Back | Close
Full Screen / Esc

Printer-friendly Version

Interactive Discussion

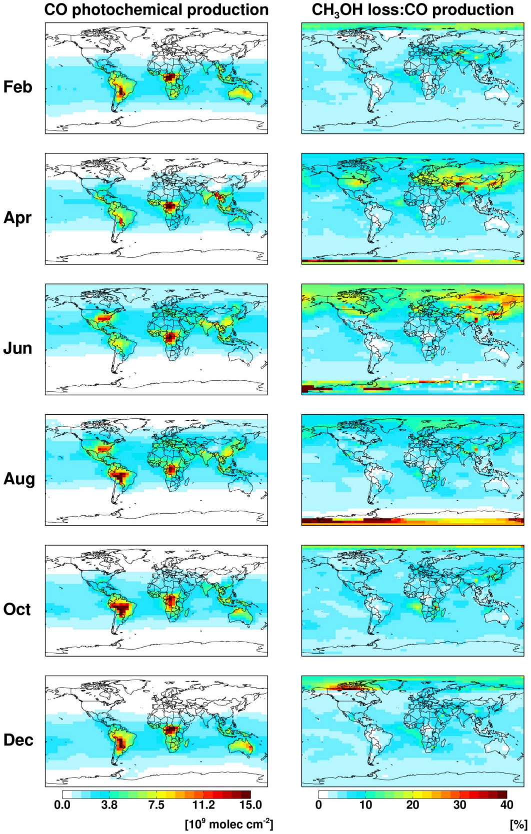

Fig. 13. Importance of methanol as a photochemical precursor of CO and HCHO. Left column: column-integrated photochemical production of CO. Right column: percent contribution from methanol oxidation in the GEOS-Chem a posteriori simulation for February, April, June, August, October, and December 2008. The fractional contribution to HCHO production is similar, since almost all photochemical production of CO goes through HCHO.